JPE 17-5-14

https://doi.org/10.6113/JPE.2017.17.5.1268
ISSN(Print): 1598-2092 / ISSN(Online): 2093-4718

Investigation of the Voltage Collapse Mechanism in Three-Phase PWM Rectifiers

Chunguang Ren*, Huipeng Li**, Yu Yang***, Xiaoqing Han†, and Peng Wang****

*,†Shanxi Key Lab of Power System Operation and Control, Taiyuan University of Technology, Taiyuan, China
**State Grid Shanxi Electric Power Research Institute, Taiyuan, China
***Shanxi Electric Power Corporation, Taiyuan, China
****Nanyang Technological University, Singapore

Abstract

Three-phase pulse width modulation (PWM) rectifiers are usually designed under the assumption of ideal ac power supply and input inductance. However, non-ideal circuit parameters may lead to a voltage collapse of PWM rectifiers. This paper investigates the mechanism of voltage collapse in three-phase PWM rectifiers. An analytical stability boundary expression is derived by analyzing the equilibrium point of the averaging state space model, which can not only accurately locate the voltage collapse boundary in the circuit parameter domain, but also reveal the essential characteristic of the voltage collapse. Results are obtained and compared with those of the trial-error method and the Jacobian method. Based on the analysis results, the system parameters can be divided into two categories. One of these categories affects the critical point, and other affects only the instability process. Furthermore, an effective control strategy is proposed to prevent a vulnerable system from being driven into the instability region. The analysis results are verified by the experiments.

Key words: Non-ideal circuit parameters, Stability boundary, Three-phase PWM rectifiers, Voltage collapse

I. INTRODUCTION

Three-phase voltage-source pulse width modulation (PWM) rectifiers have been increasingly employed for high-performance applications such as uninterrupted power supplies, distributed generations and battery energy storage systems [1]-[3].

The operation and control of three-phase PWM rectifiers are usually analyzed under the assumption of ideal ac power supply and input inductor [4]. However, the ac circuit of a practical PWM rectifier, which is usually connected to a low voltage distribution network, has a large series resistance from the distribution network and input inductance. A large total series resistance may lead to system instability of three-phase PWM rectifiers [5].

Most studies have focused on improving the performance of three-phase PWM rectifiers [6]-[9]. Stability problems of three-phase PWM rectifiers under the condition of an ideal ac power supply have been investigated in [10]-[12]. The effects of grid impedance on the stability of three-phase PWM converters have recently become a significant topic [13]-[23]. Impedance based methods applying the Nyquist criterion are commonly used to investigate the dynamic interactions between the grid impedance and three-phase PWM converters [14]-[19]. The instabilities caused by impedance incompatibility between the PWM converter and the ac source are studied in [15], [16]. The results of these studies show that source-side dynamics can negatively interact with PWM converters, which results in distortions of the point of common coupling (PCC) voltage and input current. M. Céspedes and J. Sun extended the impedance-based stability analysis method to a more general unbalanced three-phase system characterized by couple sequence impedances [17], [18]. The coupling effect due to the grid impedance between paralleled grid-connected PWM converters has been described in [19], [20]. Although the impedance-based

Manuscript received Nov. 7, 2016; accepted Jun. 4, 2017
Recommended for publication by Associate Editor Yong Kang.
†Corresponding Author: hanxiaoqing@tyut.edu.cn
Tel: +86-0351-6014920, Taiyuan University of Technology
*Shanxi Key Lab of Power System Operation and Control, Taiyuan University of Technology, China
**State Grid Shanxi Electric Power Research Institute, China
***Shanxi Electric Power Corporation, China
****Nanyang Technological University, Singapore

method is suitable to resolve system impedance incompatibilities, it is actually based on small-signal linear models in the frequency domain [21]. As a result, the internal dynamics and nonlinear phenomena were disregarded.

The averaging state space model is another normal method which can be applied to study the instability caused by complex system interactions [22]-[26]. The low-frequency instability phenomena in three-phase PWM converters connected to non-ideal grids with a large inductive impedance have been studied [22], [23]. Jacobian method obtained from an averaging state space model was used to identify the instability. The results show that the system looses stability via a Hopf bifurcation. The unstable oscillation of a matrix converter has been studied [25]. It concluded that there is no large reactive component in a matrix converter topology used to buffer energy, which leads to oscillations of the voltages and currents. The impact of a dc load disturbance on the catastrophic bifurcation of a PWM rectifier has been studied [26]. Simulation and test results show that a larger dc load might lead to system instability. Although an averaging state space model is suitable to analyze the nonlinear operation of a converter circuit, it cannot produce a compact analytical model to provide qualitative information and insight. In addition, the existing research on the critical point of the voltage collapse in three-phase PWM rectifiers always involves the control parameters and input inductance. As a result, the inherent instability characteristic behind the voltage collapse phenomena is ignored.

In this paper, the stability boundary and voltage collapse mechanism of three-phase PWM rectifiers are analyzed. An analytical expression is obtained by considering the inherent circuit state equations. The voltage collapse point obtained by this analytical expression is consistent with the stability boundary obtained by the trial-error method and the Jacobian method. A simplified circuit model is proposed to illustrate the origin of the voltage collapse based on the maximum power transfer. The effects of various circuit parameters on the voltage collapse are identified in detail and an effective measure is proposed to avoid instability.

This paper is organized as follows. Section II presents the phenomena of voltage collapse by simulations. In section III, nonlinear state equations of the closed-loop PWM rectifier are derived. In section IV, the stability boundary and the voltage collapse mechanism for the rectifier are analyzed from different aspects of the system dynamic. Section V describes the dynamic process of instability. In section VI, the parameters related to the voltage collapse phenomena are classified, and an effective protection measure is proposed. In section VII, some experiments have been carried out to verify the theoretical analysis. Section VIII concludes this paper.

II. VOLTAGE COLLAPSE OF A PWM RECTIFIER

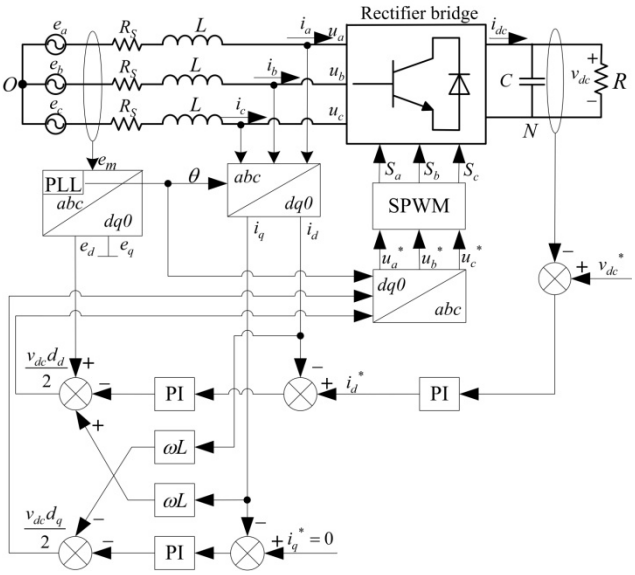

Fig. 1. Three-phase PWM rectifier control block diagram.

TABLE I
PARAMETERS OF THE PWM RECTIFIER

parameter	e_m/V	L/H	C/F	R/Ω	v^*_{dc}
value	220	0.003	0.001	10	600
parameter	K_{vp}	K_{vi}	K_{cp}	K_{ci}	f_s/kHz
value	0.02	9	10	100	10

The dual-loop control block of a PWM rectifier shown in Fig. 1 is used to analyze system stability issues, where e_S (s=a, b, c) represents the ac source, L is the filter inductance, and R_S denotes the total equivalent series resistance on the ac side of the rectifier. The parameters of the rectifier are shown in Table I. The voltage collapse phenomena and the corresponding R_S are investigated using Matlab simulation through the trial-error method.

When R_S≤1.00Ω, the rectifier operates in the stable condition with a constant dc voltage and a unity power factor. When R_S reaches 1.01Ω, the voltage collapse occurs. Fig. 2 shows transient waveforms of the dc voltage v_{dc} and the phase current i_a. Fig. 2(a) shows that the dc voltage keeps constant before 3.2s, starts to drop at 3.2s, and reduces to zero at about 3.4s. The transient process can be observed in detail in Fig. 2(b). The current i_a increases continuously from the initial value, reaches to a peak value of 300A at 3.2s, and then drops to 225A at 3.4s, which is 60% larger than the normal stable current 140A. i_a also lags the grid voltage e_a, and the system loses stability.

Fig. 3 shows the three PWM switching signals of the rectifier after the voltage collapse. It can be seen from Fig. 3 that the switching signals $S_aS_bS_c$ present six combinations and that the switching frequency becomes 50Hz, which is far away from the normal carrier signal frequency of 10 kHz. When $S_aS_bS_c$=101, the circuit diagram of the rectifier is shown in Fig. 4. It can be seen that the currents only circulate

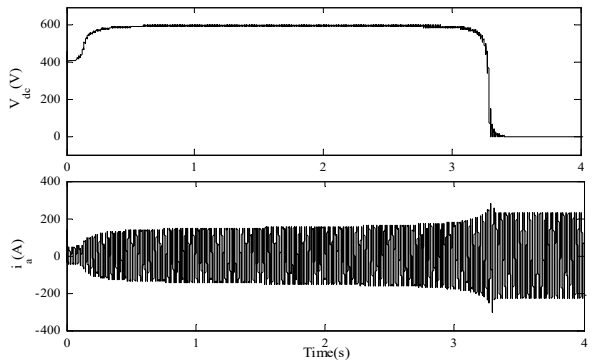

(a)

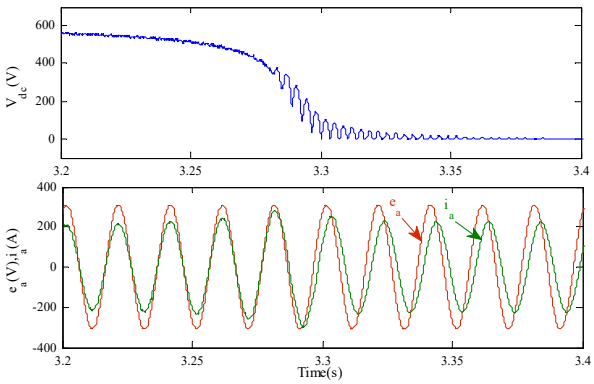

(b)

Fig. 2. Simulation results showing voltage collapse phenomena for R_S=1.01Ω. (a) Transient waveforms of v_{dc} and i_a, and (b) the local close-up waveforms of v_{dc}, e_a and i_a.

among three phases through R_S and L, and that there is no dc output current which leads to the dc voltage collapse to zero. The other switching states have the similar results. Fig. 5 shows the critical points and the corresponding R_S and R. It can be seen that there is a linear relationship between R_S and R. The slop can be calculated as 0.1010. The maximum load that can be supplied reduces with the increase of R_S.

III. State Equation of the PWM Rectifier

Although the instability of a PWM rectifier can be simulated using the trial-error method, the relationship between the circuit parameters and the instability cannot be explicitly represented and interpreted. A longer simulation time is required to determine the value of R_S for the voltage collapse. Therefore, the quantitative relationship between the critical point and R_S is important for the design of the PWM rectifier.

The instability phenomena can be analyzed based on the state equations of the closed-loop system shown in Fig. 1. The time domain differential equations of the rectifier in the three-phase stationary coordinate are depicted as:

$$L\frac{di_k}{dt} = e_k - R_S i_k - v_{dc}\frac{d_k}{2} + \frac{v_{dc}}{3}\sum_{k=a,b,c}\frac{d_k}{2} \quad (1)$$

$$C\frac{dv_{dc}}{dt} = \sum_{k=a,b,c}\frac{d_k i_k}{2} - \frac{v_{dc}}{R} \quad (2)$$

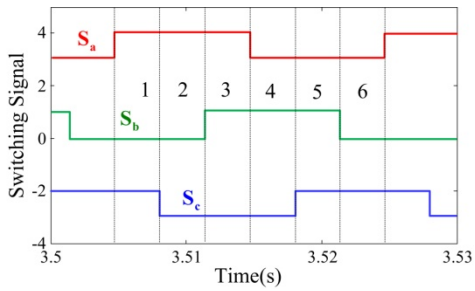

Fig. 3. Switching signals of the rectifier after a voltage collapse.

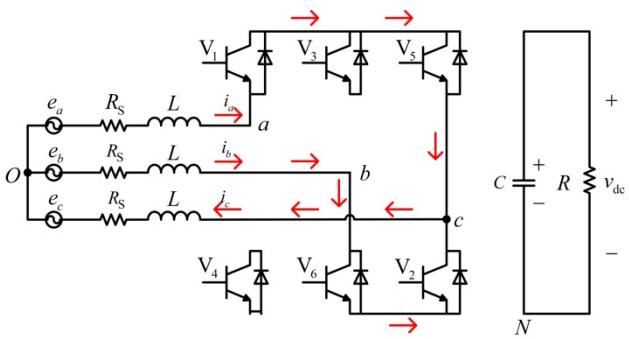

Fig. 4. Circuit diagram when $S_aS_bS_c$ =101.

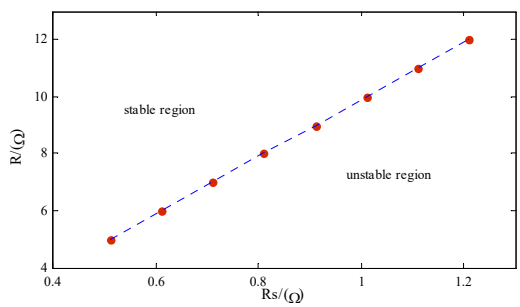

Fig. 5. Critical points and the corresponding R_S and R.

where d_k is the duty cycle of the switching function S_k. S_k=1 means that the upper arms turn on and the lower arms shut down, while S_k=-1 means the opposite.

When the d-axis is selected in the same direction as the voltage source e_a, the state equations of (1) and (2) in the d-q synchronous rotating coordinate can be derived as:

$$L\frac{di_d}{dt} = e_d + \omega L i_q - R_S i_d - v_{dc}\frac{d_d}{2} \quad (3)$$

$$L\frac{di_q}{dt} = e_q - \omega L i_d - R_S i_q - v_{dc}\frac{d_q}{2} \quad (4)$$

$$C\frac{dv_{dc}}{dt} = \frac{1}{2}\left(d_d i_d + d_q i_q\right) - \frac{v_{dc}}{R} \quad (5)$$

where d_d and d_q are the duty cycle in the d-q axis, and i_d and i_q represent the d-q currents.

According to the control block shown in Fig.1, the state equations of the dual-loop control system can be derived. The outer voltage loop state equation can be expresses as:

$$\frac{dx_1}{dt} = v_{dc}^* - v_{dc} \quad (6)$$

$$i_d^* = K_{vp}(v_{dc}^* - v_{dc}) + K_{vi}x_1 \quad (7)$$

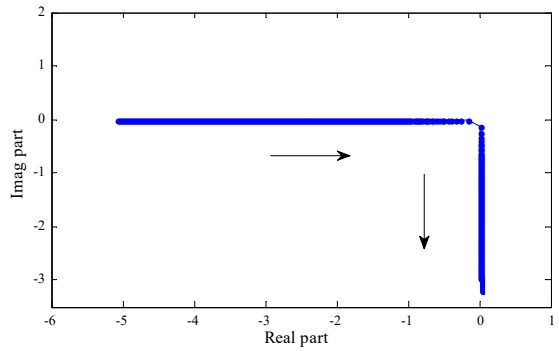

Fig. 6. Root locus of an eigenvalue moving from the left toward zero when R_S increases.

where K_{vp} and K_{vi} are the proportional and integral coefficients of the outer voltage loop, respectively.

The inner current loop state equations are expressed as:

$$\frac{dx_2}{dt} = i_d^* - i_d \tag{8}$$

$$(\frac{v_{dc}}{2} d_d)^* = e_d - K_{cp}(i_d^* - i_d) - K_{ci}x_2 + \omega L i_q \tag{9}$$

$$\frac{dx_3}{dt} = i_q^* - i_q \tag{10}$$

$$(\frac{v_{dc}}{2} d_q)^* = e_q - K_{cp}(i_q^* - i_q) - K_{ci}x_3 - \omega L i_d \tag{11}$$

where K_{cp} and K_{ci} are the proportional and integral coefficients of the inner current loop, respectively.

The normalized form of the state equations of (3)-(6), (8) and (10) can be written as:

$$\dot{\boldsymbol{x}} = \boldsymbol{f(x)} \tag{12}$$

where $\boldsymbol{x} = [x_1 \quad x_2 \quad x_3 \quad i_d \quad i_q \quad v_{dc}]^T$ is state vector for the state variables, and $\boldsymbol{f(x)} = [f_1 \quad f_2 \quad f_3 \quad f_4 \quad f_5 \quad f_6]^T$ is the vector of the nonlinear functions (3)-(6), (8) and (10). Obviously, the state equations are nonlinear due to the quadratic items of the state functions. The state equations are the basis for solving the stability problem of nonlinear systems.

IV. Stability Boundary and Voltage Collapse Mechanism

The stability boundary and voltage collapse mechanism for the rectifier can be analyzed from different perspective of the system dynamic.

A. Eigenvalue Analysis

In this method, system stability is determined by the eigenvalues of the Jacobian matrix at the equilibrium point of a nonlinear system. Setting $\boldsymbol{f(x)=0}$, the equilibrium point of the rectifier are calculated as:

$$\boldsymbol{x_0} = \begin{cases} x_{10} = \dfrac{e_d - \sqrt{e_d^2 - 4R_S v_{dc}^2/R}}{2R_S k_{vi}}, x_{20} = \dfrac{e_d - \sqrt{e_d^2 - 4R_S v_{dc}^2/R}}{2k_{ci}}, x_{30} = 0 \\ i_{d0} = \dfrac{e_d - \sqrt{e_d^2 - 4R_S v_{dc}^2/R}}{2R_S}, i_{q0} = 0, v_{dc0} = V_{dc}^* \end{cases}$$

TABLE II
Eigenvalues of the Rectifier with a Varying R_S

R_S	Eigenvalues	Stability
0.990Ω	-3517.2, -4.10691, -193.98, -92.535, -3570.0, -93.372	Stable
1.000Ω	-3519.1, -2.7331, -194.53, -92.578, -3573.4, -93.282	Stable
1.008Ω	-3518.8, -0.54342, -195.37 -92.722, -3576.1, -93.210	Stable
1.010Ω	-3518.8-1.9049i, 0-1.2133i, -195.59+0.4443i, -92.759+0.1174i, -3576.8, -93.192	Unstable
1.020Ω	-3.522.7-4.9807i, 0-3.2081i, -195.65+1.1772i, -92.682+0.3142i, -3580.2, -93.104	Unstable

The Jacobian matrix $\boldsymbol{J(x)}$ of (12) at the equilibrium point is derived as:

$$\boldsymbol{J}(x) = \begin{bmatrix} 0 & 0 & 0 & 0 & 0 & -1 \\ K_{vi} & 0 & 0 & -1 & 0 & -K_{vp} \\ 0 & 0 & 0 & 0 & -1 & 0 \\ \dfrac{K_{vi}K_{cp}}{L} & \dfrac{K_{ci}}{L} & 0 & \dfrac{-K_{cp}-R_S}{L} & 0 & -\dfrac{K_{vp}K_{cp}}{L} \\ 0 & 0 & \dfrac{K_{ci}}{L} & 0 & \dfrac{-K_{cp}-R_S}{L} & 0 \\ -\dfrac{K_{vi}K_{cp}i_{d0}}{C_{dc}v_{dc}} & -\dfrac{K_{ci}i_{d0}}{C_{dc}v_{dc}} & -\dfrac{K_{ci}i_{q0}}{C_{dc}v_{dc}} & J_{64} & J_{65} & J_{66} \end{bmatrix}$$

where $J_{64} = \dfrac{1}{C_{dc}v_{dc}}\left(e_d + 2K_{cp}i_{d0} + K_{vp}K_{cp}v_{dc0} - K_{vp}K_{cp}v_{dc}^* - K_{vi}K_{cp}x_{10} - K_{ci}x_{20}\right)$

$J_{65} = \dfrac{1}{C_{dc}v_{dc}}\left(e_q - K_{cp}i_q^* + 2K_{cp}i_{q0} - K_{ci}x_{30}\right)$

$J_{66} = \dfrac{1}{C_{dc}v_{dc0}^2}\left(K_{vi}K_{cp}i_{d0}x_{10} + K_{ci}i_{d0}x_{20} + K_{ci}i_{q0}x_{30} - i_{d0}\left(e_d + K_{cp}i_{d0} - K_{vp}K_{cp}v_{dc}^*\right)\right)$

$-\dfrac{i_{q0}}{C_{dc}v_{dc}^2}\left(e_q - K_{cp}i_q^* + K_{cp}i_{q0}\right) - \dfrac{1}{C_{dc}R}$

The eigenvalues for different values of R_S can be obtained from the Jacobian matrix $\boldsymbol{J(x)}$ by numerical calculations. Table II shows a typical scenario for variations of the eigenvalues. It can be observed that all of the eigenvalues are negative real numbers when R_S<1.0Ω. When R_S (1.0Ω<R_S<1.008Ω) increases, the second eigenvalue moves from negative toward the origin along the real axis. When R_S=1.008Ω, the second eigenvalue is much closer to zero. Further increases of R_S (R_S>1.009Ω) lead to the movement of the second eigenvalue along the imaginary axis from zero to negative, and system becomes unstable. When R_S=1.01Ω, the second eigenvalue is -1.2133i. The locus of the second eigenvalue is plotted in Fig. 6, which is a typical characteristic of a saddle-node bifurcation. This means that the system may lose its stability via a saddle-node bifurcation, resulting in a voltage collapse of the rectifier, which is fully coincident with the simulation results shown in Fig. 2.

B. System Equilibrium Point Analysis

Voltage collapses are often be linked with the loss of the stable bounded solutions of a nonlinear system modeled by

(12) near the critical operation condition [27]. However, the critical points calculated by Jacobian methods cannot fully reflect the characteristics of a structurally unstable system, and they cannot provide an analytical solution. The stability boundary of a rectifier is analyzed by the static bifurcation theory [28] in this section. An analytical solution of the stability boundary can be obtained solely from the inherent circuit state equations. Setting the derivatives of (3)-(5) to zero, the steady state circuit equations of the circuit are obtained as:

$$U_d = \frac{V_{\rm dc}}{2} D_d = V_m \cos\alpha = \sqrt{3} e_m - R_{\rm S} I_d \tag{13}$$

$$U_q = \frac{V_{\rm dc}}{2} D_q = V_m \sin\alpha = -\omega L I_d \tag{14}$$

$$\frac{V_{\rm dc}}{R} = \frac{1}{2} D_d I_d \tag{15}$$

where I_d and I_q are the steady state values of i_d and i_q, respectively, and U_d and U_q are the terminal voltages of the rectifier in the *d-q* axis.

Substituting D_d from (15) into (13):

$$R_{\rm S} I_d^2 - \sqrt{3} e_m I_d + V_{\rm dc}^2 / R = 0 \tag{16}$$

The system stability region can be determined by the roots of the quadratic equation of I_d.

When $\Delta = 3e_{\rm m}^2 - 4R_{\rm S}V_{\rm dc}^2 / R < 0$, (16) has no real root, i. e. the rectifier has no equilibrium point. Thus, the system is not stable.

When $3e_{\rm m}^2 - 4R_{\rm S}V_{\rm dc}^2 / R > 0$ (i.e., $0 \le R_{\rm S} < 3e_{\rm m}^2 R / 4V_{\rm dc}^2$), there are two distinct real roots:

$$\begin{cases} I_{d1} = \dfrac{\sqrt{3} e_m - \sqrt{3{e_m}^2 - \dfrac{4{V_{dc}}^2 R_S}{R}}}{2R_S} \\ I_{d2} = \dfrac{\sqrt{3} e_m + \sqrt{3{e_m}^2 - \dfrac{4{V_{dc}}^2 R_S}{R}}}{2R_S} \end{cases} \tag{17}$$

In this case, the system stability can be determined by the partial derivative of (16) with respect to I_d.

$$\frac{\partial f(I_d, R_S)}{\partial I_d} = \pm\sqrt{3{e_m}^2 - \frac{4{V_{dc}}^2 R_S}{R}} \tag{18}$$

When $-\sqrt{3{e_m}^2 - 4{V_{dc}}^2 R_S / R} < 0$, I_{d1} is a convergence equilibrium point. When $\sqrt{3{e_m}^2 - 4{V_{dc}}^2 R_S / R} > 0$, I_{d2} is a divergence equilibrium point. Fig. 7 shows the bifurcation curve with respect R_S. It is obvious that the system losses stability through saddle-node bifurcation and the bifurcation point is $R_{\rm S} = 3e_{\rm m}^2 R / 4V_{\rm dc}^2$ ($I_d = 2V_{\rm dc}^2 / \sqrt{3} e_m R$).

The stability boundary of R_S is obtained as:

$$0 \le R_{\rm S} \le 3e_{\rm m}^2 R / 4V_{\rm dc}^2 \tag{19}$$

For the rectifier with the parameters in Table I, the boundary of R_S for stable operation can be obtained as

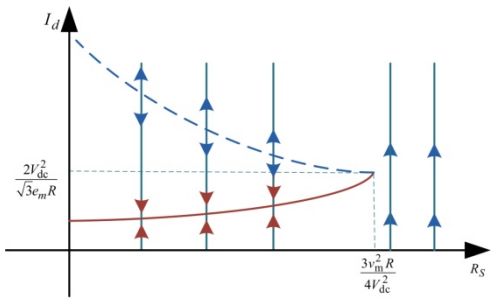

Fig. 7. Curve of I_d versus R_S, and the corresponding bifurcation point.

$R_S \le 1.008\Omega$, which is the same as the results obtained in section IV-A.

According to (19), the linear relationship between R_S and R in the bifurcation point can be represented. The slope can be expressed as $R_{\rm S}/R = 3e_{\rm m}^2 R / 4V_{\rm dc}^2$, and it is 0.1008 with the parameters in Table I, which is much closer to the value of 0.1010 obtained by simulation in section II. Moreover, equation (19) can be used to determine not only the voltage collapse boundaries for different parameters, but also the analytical relationship between the various parameters affecting the critical point.

It can be noticed that the system equilibrium point $\boldsymbol{x_0}$ in the Jacobian matrix $\boldsymbol{J(x)}$ is determined by the stability boundary expression (19). This result further illustrates that the essence of the voltage collapse of the rectifier is a saddle-node bifurcation.

In addition, equation (19) also shows the limit of the dc load disturbance for the system stability.

$$R \ge 4R_S V_{dc}^2 / 3e_{\rm m}^2 \tag{20}$$

Therefore, Equation (20) can be used to predict the voltage collapse phenomenon in three-phase PWM rectifiers caused by load disturbances.

C. Circuit Principle for Voltage Collapse

The active power transferred to the rectifier bridge at the equilibrium point is:

$$P = U_d I_d + U_q I_q = U_d I_d \tag{21}$$

The reactive power transferred to the rectifier is:

$$Q = U_d I_q - U_q I_d = -U_q I_d = \omega L {I_d}^2 \tag{22}$$

Considering (13), (14), (21) and (22), the ac side of the rectifier can be represented by an equivalent impedance $Z_p = R_p + X_p$, where:

$$R_p = \frac{U_d}{I_d} = \frac{e_d - R_S I_d}{I_d} \tag{23}$$

$$X_p = U_q / I_d = -\omega L \tag{24}$$

The equivalent circuit of the dc side of the rectifier can be represented by a dc current source. The equivalent circuit of the system is shown in Fig. 8.

According to the maximum power transfer theorem, the

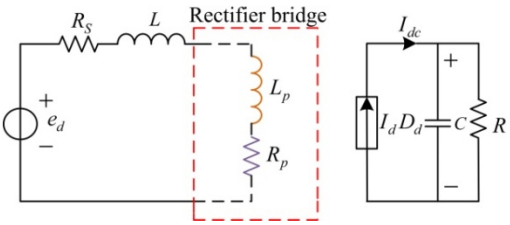

Fig. 8. Simplified equivalent circuit of the rectifier at the equilibrium point.

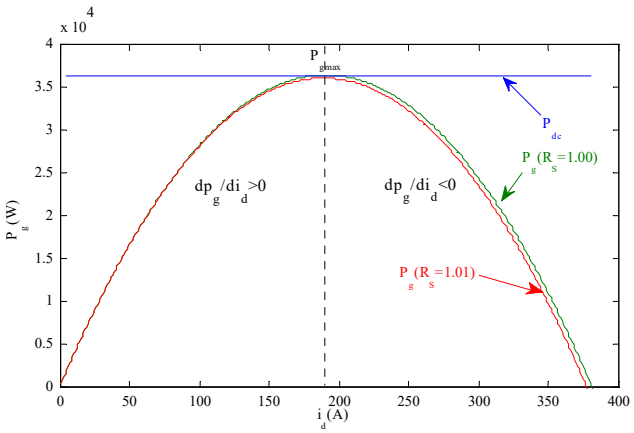

Fig. 9. Curves of the input power versus the active current.

maximum average active power transformed by the rectifier is calculated as $P_{g\max} = e_d^2 / 4R_S$ [29].

The active power delivered from a source to the rectifier while considering the loss of the equivalent impedance R_S can be expressed as:

$$P_g = -R_S I_d^2 + \sqrt{3} e_m I_d \tag{25}$$

For stable operation, the input power to the rectifier and the output power to the dc load must be balanced as:

$$P_{dc} = \frac{V_{dc}^2}{R} = P_g \tag{26}$$

Fig. 9 shows curves of P_{dc} and P_g which are obtained from (25) and (26) based on the parameters in Table I. It can be seen that the system input power changes based on R_S and i_d. When $R_S \leq 1.00\Omega$, the input power curve intersects with the dc load curve. In this case, the system reaches stable operation at the left insertion point of the two curves. When $R_S \geq 1.01\Omega$, the input power curve does not intersect with the dc load curve. This means that the system cannot reach a stable operation before dP_g/di_d changes from positive into negative.

Accordingly, the following should be satisfied:

$$P_{g\max} = \frac{e_d^2}{4R_S} \geq \frac{V_{dc}^2}{R} \tag{27}$$

Substituting $e_d = \sqrt{3} e_m$ into (27) yields:

$$3e_m^2 - 4R_S V_{dc}^2 / R \geq 0 \tag{28}$$

It is obvious that (28) is the same as (19). Equation (27) further proves that R_S is the key parameter for the voltage collapse of a rectifier. The active power transformed from the rectifier to the dc load is constrained by R_S. When the dc load is over the transfer limit of the active power, the system operates into the nonlinear region, which finally leads to a dc voltage collapse.

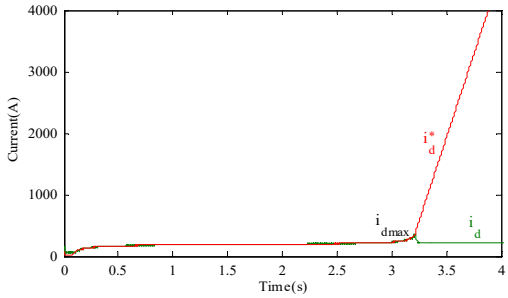

Fig. 10. Curve of the active current and its reference value.

In addition, equation (24) is true if the system is stable and there is no over-modulation. It can be concluded from the above analysis that the voltage collapse boundary of the rectifier is not affected by the line inductance L.

V. Dynamic Process of a Voltage Collapse

As shown in Fig. 9, when the input power curve does not intersect with the load curve below P_{gmax}, the active current still increases in the promotion of the outer voltage loop. However, the input power starts to decrease with a further increase of the current i_d, and there is insufficient power for the load demand. For a larger $(v_{dc}^* - v_{dc})$, the following formula can be obtained from (7).

$$\frac{di_d^*}{dt} = K_{vp} \frac{d(v_{dc}^* - v_{dc})}{dt} + K_{vi} \frac{dx_1}{dt} > 0 \tag{29}$$

Equation (29) shows that i_d^* always increases with t. However, i_d has a maximum value i_{dmax}, as shown in Fig. 10. i_{dmax} can be obtained from (25) as:

$$i_{d\max} = \frac{\sqrt{3} e_m}{2R_S} \tag{30}$$

When i_d^* becomes larger than i_{dmax}, i_d can no longer follow i_d^* due to the nonlinear characteristic of the circuit. It is finally stable at a certain value, as shown in Fig. 10. i_q is similar to i_d. When the system is stable, $Ldi_d/d_t = Li_q/d_t = 0$. This is common with a symmetrical three-phase supply voltage, namely, $e_q = 0$. Considering that $v_{dc} = 0$, combine these conditions with (3)-(4). Equation (31) can be obtained as:

$$\begin{cases} \lim\limits_{t \to +\infty} i_d = R_S e_d / ((\omega L)^2 + R_S^2) \\ \lim\limits_{t \to +\infty} i_q = -\omega L e_d / ((\omega L)^2 + R_S^2) \end{cases} \tag{31}$$

In this case, the value of $(i_d^* - i_d)$ will be much larger, i.e. $\lim\limits_{t \to +\infty} (i_d^* - i_d) = \infty$. According to (9), $\lim\limits_{t \to +\infty} (\frac{v_{dc}}{2} d_d)^* = -\infty$. Then (32) can be obtained as:

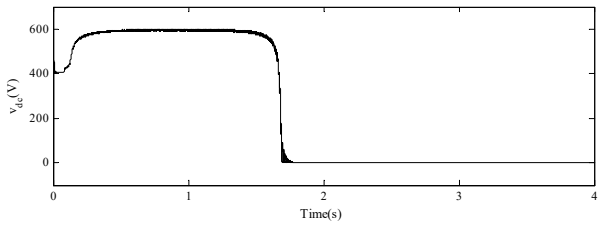

(a)

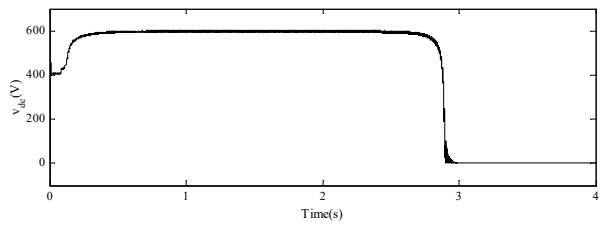

(b)

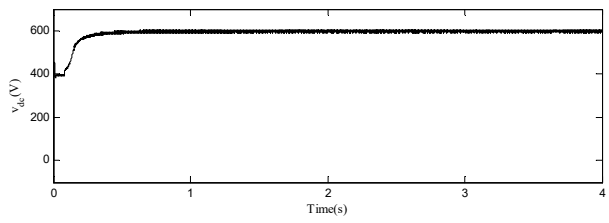

(c)

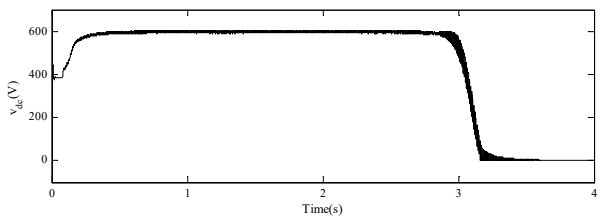

(d)

Fig. 11. Simulation results of a rectifier under different parameters; (a) waveform of the dc voltage for L=0.003H, R_S=1.02Ω, K_{vi}=9; (b) for L=0.003H, R_S=1.01Ω, K_{vi}=10; (c) for L=0.006H, R_S=1.00Ω, K_{vi}=9; (d) for L=0.006H, R_S=1.01Ω, K_{vi}=9.

$$\lim_{t\to+\infty}\left|u_k^*\right| = \lim_{t\to+\infty}\sqrt{\left[\left(\frac{v_{dc}}{2}d_d\right)^*\right]^2+\left[\left(\frac{v_{dc}}{2}d_q\right)^*\right]^2} = \infty \quad (32)$$

where u_k^* (k=a, b, c) are modulation signals. At this time, the amplitude of the modulated signal is far larger than the amplitude of the carrier, which leads to the switching frequency becoming 50Hz, as shown in Fig. 3. In addition, the circuit diagram presents as Fig. 4.

VI. Parameter Impacts on a Voltage Collapse

According to the former analysis, the parameters related to the critical point of the voltage collapse are shown in (19). The other parameters do not affect the critical point of the rectifier. However, they may affect the instability process. In this section, the impacts of parameters on the instability process are analyzed. Based on the analysis results, the parameters related to the voltage collapse phenomena can be classified. In addition, a protective measure is proposed.

TABLE III
Parameter Classification

Affect the critical point				Affect only the process				
e_m	v^*_{dc}	R	R_S	K_{vp}	K_{vi}	K_{cp}	K_{ci}	L

A. Effect of R_S

R_S not only determines the critical point, but also affects the instability process when it beyond the limit defined by (19). In Fig. 11 (a), when R_S increase to 1.02Ω, the system becomes unstable at 1.7s. Compared with the transient time 3.2s shown in Fig. 2, the system loses stability much faster with the increase of R_S. The maximum power point P_{gmax} of the rectifier decreases with the increases of R_S. Therefore, the rectifier reaches P_{gmax} in a shorter time, which leads to the system lose stability much faster.

B. Effect of the Control Parameters

In Fig. 11 (b), when K_{vi} increases to 10, the rectifier becomes unstable at 2.9s, which is less than 3.2s, as shown in Fig. 2. This means that the unstable operation starts early when K_{vi} increases. This is because i_d raises fast due to increases of K_{vi}. Therefore, the rectifier has a shorter time to reach the maximum power point P_{gmax}. The duration of the system stable operation will be shortened accordingly. K_{vp} has the same results as K_{vi}. Similarly, with the outer voltage loop, larger values of K_{cp} and K_{ci} accelerate the action of the inner current loop, which results in a voltage collapse of the rectifier in a shorter time.

C. Effect of the Inductance L

When R_S=1.00Ω, which is very close to the critical point 1.008, the system response for L=0.006H is shown in Fig. 11 (c). It can be seen from Fig. 11 (c) that the dc voltage is kept constant and that the rectifier is stable. When R_S=1.01Ω, which is larger than the critical value, the rectifier operates in the unstable condition. It can be seen from Fig. 11 (d) that the rectifier is kept stable for nearly 3s for L=0.006H. Comparing these results with those in Fig. 2, a larger inductance can accelerate the inherent instability of the system. If the other parameters remain constant, a larger inductance L accelerates the increase of the modulated signals u_k^* (k=a, b, c), which shortens the transient time for a voltage collapse of the rectifier.

According to the above analysis, the parameters of the rectifier related to the voltage collapse phenomena can be divided into two categories as shown in Table III. The parameters shown in (19) affect the critical point, and the others affect only the process of the voltage collapse.

D. Protective Measures for a Voltage Collapse

Based on the above analysis, the parameters that affect the critical point of a voltage collapse have been shown in Table

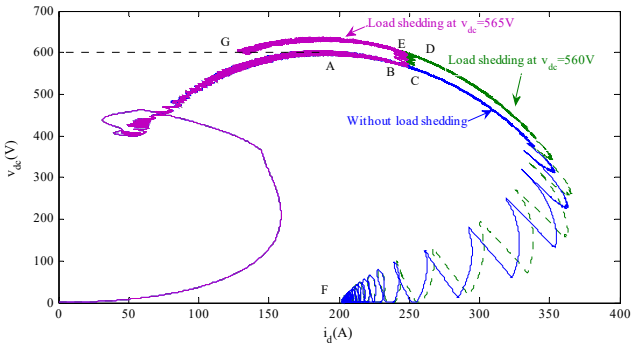

Fig. 12. Phase portraits of the dc voltage and active current with and without load shedding.

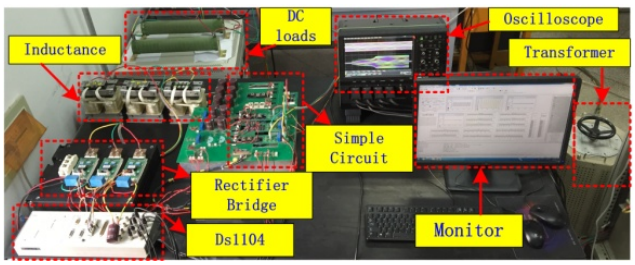

Fig. 13. Experiment platform of the proposed rectifier.

III. It can be concluded that the dc load R is the only available parameter to prevent a rectifier from a voltage collapse under certain conditions. Therefore, load shedding can be used as an effective protection. Simulation and test results show that load shedding before the dc voltage reaches zero can restore a rectifier back to normal operation.

Fig. 12 shows the dynamic response of a rectifier with the parameters shown in Table I. When R_S=1.01Ω, the system operates along the curve $\overset{\frown}{\text{ABCF}}$ and ends at F after a period of fluctuation as a voltage collapse occurs. The system loses stability without load shedding. If the same load is curtailed at a different time in the process of dc voltage drops, the rectifier shows different responses. When a 3.6kW load is curtailed when the dc voltage drops to 565V, the system operates along the curve $\overset{\frown}{\text{ABEG}}$ and restores stability at point G. However, a 3.6kW load shedding cannot drive the system back to stability when the dc voltage decreases to 560V and the system eventually operates along the curve $\overset{\frown}{\text{ACDF}}$ to F. Simulations show that more load curtailment is required to drive a system to a normal equilibrium point if the load is curtailed at the moment of the lower dc voltage.

VII. Experimental Verification

The stability boundary derived by the proposed methods is verified by a laboratory setup. Insulated gate bipolar transistor (IGBT) modules from *Infineon* (FF225R17ME4) are used.

The rectifier is interfaced to the utility grid (380V line-line rms) through a 220V/30V step-down transformer. The

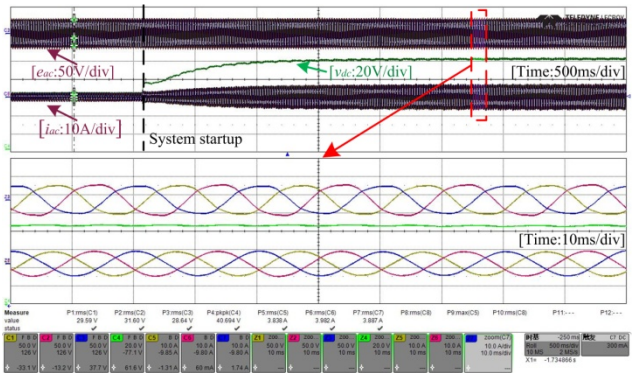

(a)

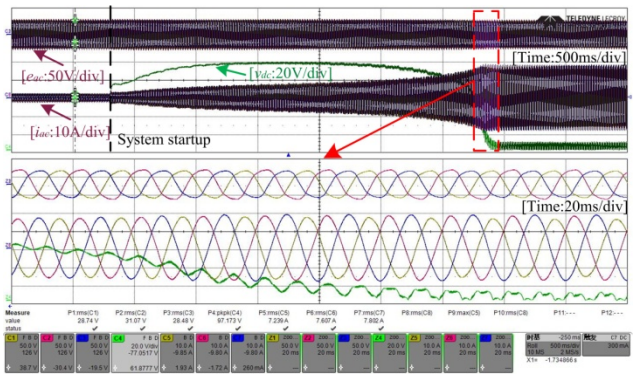

(b)

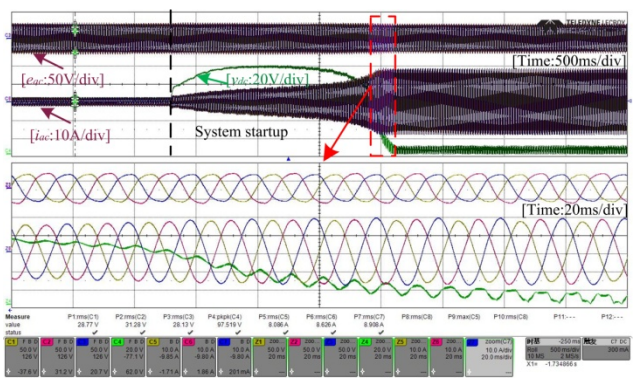

(c)

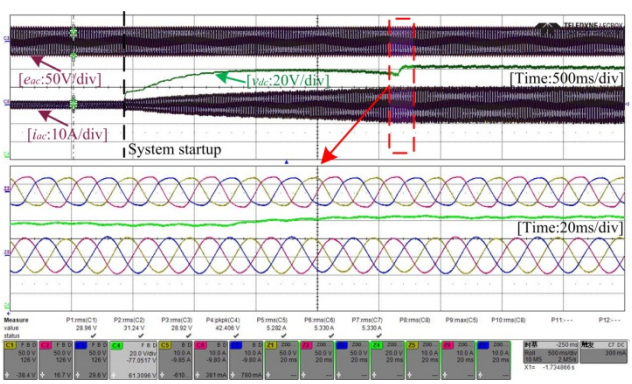

(d)

Fig. 14. Experiment waveforms of the dc voltage v_{dc}, ac voltage e_{ac} and ac current i_{ac}: (a) for R_S=2.65Ω, K_{vi}=9; (b) for R_S=2.75Ω, K_{vi}=9; (c) for R_S=2.75Ω, K_{vi}=11; (d) for a 50W load is curtailed after the dc voltage starts to drop.

parameters of the circuit are e_m=30V, L=3mH, C=1000uF, R=40Ω and V^*_{dc}=100V. The parameters of the control system are K_{vp}=0.02, K_{vi}=9, K_{cp}=10, K_{ci}=100 and f_s=10 kHz. Considering the fact that the system needs to operate in the fault mode, the rectifier power is set to 1kW due to the limitations of the passive components. However, this does not affect the conclusion.

The series resistances in the ac input circuit are measured. The inductor resistance is 0.15Ω, the on-resistance of the IGBT is 0.03Ω, the cable resistance is 0.27Ω and source resistance is 0.315Ω. The total circuit resistances R_t is 0.765Ω. A variable resistor R_v is connected to the ac circuit to observe the voltage collapse. The experiment results are measured by an oscilloscope from Teledyne Lecroy. The experimental platform is shown in Fig. 13.

Test results of the rectifier are shown in Fig. 14. Fig. 14(a) shows the system responses when R_S=R_t+R_v=2.65Ω. The system is switched on at t=0s. The dc voltage reaches 100V at about 1.1s and is stable after 1.1s. It can be seen from the close-up waveforms that the ac current and voltage are in phase with a unity power factor. The system is stable.

Fig. 14(b) shows the transient process of the voltage collapse when R_S=2.75Ω. The system is switched on at t=0s. It can be seen that the dc voltage reaches 100V at about 1.0s, begins to drop at about 1.7s, and falls to zero at about 3.1s. The ac current increases to a peak-to-peak value of 19A at about 3.0s and is stable at 18A at 3.1s. The system loses stability. The close-up waveforms show the steady-state results in detail. The ac current lags the voltage because the current circulates between the cables, the inductor and the IGBT.

Fig. 14(c) shows the response of the rectifier by changing K_{vi} from K_{vi}=9 to K_{vi}=11 when R_S=2.75Ω. The system is switched on at t=0s. It can be seen that the dc voltage begins to drop at about 1.0s, and falls to zero at about 1.8s. Compared to the results in Fig. 14(b), the system loses stability much faster with the increase of K_{vi}, which is consistent with the simulation results. The effects of the other parameters shown in section VI have the same results as the simulation.

Fig. 14(d) shows the rectifier response for a 50W load shedding. The system is switched on at t=0s. It can be seen that the dc voltage reaches 100V at about 1.0s, and begins to drop at about 1.7s. When the 50W load is curtailed at about 2.2s, the dc voltage restores stability at about 2.5s after a short period of transient rise and a new stable state is achieved to avoid the system collapse.

VIII. CONCLUSIONS

In a practical three-phase PWM rectifier, the equivalent resistance existing in the ac circuit may lead to a dc voltage collapse. This paper investigates the inherent mechanism behind the instability phenomena. An analytical expression has been developed to predict the critical point. The results show that the critical point of a voltage collapse is a saddle-node bifurcation point. They also show that the equivalent resistance is a key factor for the voltage collapse, which limits the active power transferred from the source to the dc load. Based on the obtained results, the parameters of the system can be divided into two categories: one of which, as shown in the analytical expression, affects the critical point, while the rest only affect the process of the voltage collapse. Finally, experimental results verify the rectifier stability boundary given by the theoretical analysis. The analysis results are useful for the control circuit design and the parameter selection of three-phase rectifiers.

ACKNOWLEDGMENT

This work was supported in part by Shanxi Key Projects of Coal Based Science and Technology (MD2014-06), in part by National Nature Science Foundation of China (U1610121), in part by Shanxi Province Key Research and Development Program (201603D421007), in part by State Grid Shanxi Electric Power Company Science and Technology Project Research (52053016000W) and in part by Project Supported by Shanxi Scholarship Council of China (2015-key project 1).

REFERENCES

[1] H. S. Krishnamoorthy, D. Rana, P. Garg, P. N. Enjeti, and I. J. Pitel, "Wind turbine generator-battery energy storage utility interface converter topology with medium-frequency transformer link," *IEEE Trans. Power Electron*., Vol. 29, No. 8, pp. 4146–4155, Aug. 2014.

[2] B. Singh, B. N. Singh, A Chandra, K. Al-Haddad, A. Pandey, and D. P. Kothari, "A review of three-phase improved power quality AC-DC converters," *IEEE Trans. Ind. Electron*., Vol. 51, No. 3, pp. 641-660, Jun. 2004.

[3] A. Moawwad, V. Khadkikar, and J. L. Kirtley, "A new P-Q-V droop control method for an interline photovoltaic (I-PV) power system" *IEEE Trans. Power Del*., Vol. 28, No. 2, pp. 658–668, Apr. 2013.

[4] G. H. Gong, M. L. Heldwein, U. Drofenik, J. Minibock, K. Mino, and J. W. Kolar, "Comparative evaluation of three-phase high-power-factor AC–DC converter concepts for application in future more electric air-craft," *IEEE Trans. Ind. Electron*., Vol. 52, No. 3, pp. 727–737, Jun. 2005.

[5] B. Wen, D. Dong, D. Noroyevich, R. Burgos, P. Mattavelli, and Z. Shen, "Impedance-based analysis of grid-synchronization stability for three-phase paralleled converters," *IEEE Trans. Power Electron*., Vol. 31, No. 1, pp. 26–38, Jan. 2016.

[6] R. P. Burgos, E. P. Wiechmann and J. Holtz, "Complex state-space modeling and nonlinear control of active front-end converters," *IEEE Trans. Ind. Electron*., Vol. 52, No. 2, pp.363 -377, Apr. 2005.

[7] M. Malinowski, M. Jasinski, and M. P. Kazmierkowski, "Simple direct power control of three-phase PWM rectifier using space vector modulation (DPC-SVM)," *IEEE Trans. Ind. Electron*., Vol. 51, No. 2, pp. 447–454, Apr. 2004.

[8] X. Guo, W. Wu, and Z. Chen, "Multiple-complex

coefficient-filter-based phase-locked loop and synchronization technique for three-phase grid-interfaced converters in distributed utility networks," *IEEE Trans. Ind. Electron*., Vol. 58, No. 4, pp. 1194–1204, Apr. 2011.
[9] P. A. Janakiraman, S. Abdul Rahman, "Linear Pulse Width Modulation Under Fluctuating Power Supply," *IEEE Trans. Ind. Electron*., Vol. 61, No. 4, pp. 1769–1773, Apr. 2014.
[10] A. Radwan, Y. Mohamed, "Analysis and active-impedance-based stabilization of voltage-source-rectifier loads in grid-connected and isolated microgrid applications," *IEEE Trans. Sustain. Energy*, Vol. 4, No. 3, pp. 563 -576, Jul. 2013
[11] J. Espinoza, G. Joós, M. Perez, and T. L. A. Moran, "Stability issues in three-phase PWM current/voltage source rectifiers in the regeneration mode," in *Proc. IEEE ISIE*, pp. 453-458, 2000.
[12] M. Liserre, A. D. Aquila, F. Blaabjerg, "Stability improvements of an LCL-filter based three-phase active rectifier," in *Proc. IEEE PESC*., pp. 1195–1201, 2002
[13] M. Liserre， R. Teodorescu， F. Blaabjerg, "Stability of photovoltaic and wind turbine grid-connected inverters for a large set of grid impedance values," *IEEE Trans. Power Electron*., Vol. 21, No. 1, pp. 263-272, Jan. 2006.
[14] J. Sun, "Impedance-based stability criterion for grid-connected inverters," *IEEE Trans. Power Electron*., Vol. 26, No. 11, pp. 3075-3078, Nov. 2011.
[15] L. Jessen, F. W. Fuchs, "Modeling of inverter output impedance for stability analysis in combination with measured grid impedances," in *Proc. IEEE PEDG*., pp. 2329-5759, Jun. 2015.
[16] A. Radwan, and Y. Mohamed, "Analysis and Active-Impedance-Based Stabilization of Voltage-Source-Rectifier Loads in Grid-Connected and Isolated Microgrid Applications," *IEEE Trans. Sustain. Energy*, Vol. 4, No. 3, pp. 563-576, Jul. 2013.
[17] M. Cespedes, J. Sun, "Impedance Modeling and Analysis of Grid-Connected Voltage-Source Converters," *IEEE Trans. Power Electron*., Vol. 29, No. 3, pp. 1254-1261, Mar. 2014.
[18] M. Céspedes, J. Sun, "Method for stability analysis of unbalanced three-phase systems," in *Proc. IEEE ECCE*., pp. 3090-3097, 2012.
[19] J. L. Agorreta, M. Borrega, J. López, and L. Marroyo, "Modeling and Control of N-Paralleled Grid-Connected Inverters With LCL Filter Coupled Due to Grid Impedance in PV Plants," *IEEE Trans. Power Electron*., Vol. 26, No. 3, pp. 770-785, Mar. 2011.
[20] C. Yoon, X. Wang, F. Silva, C. Bak, and F. Blaabjerg "Harmonic stability assessment for multi-paralleled, grid-connected inverters," *2014 Interactional Power Electronic and Application Conference and Exposition*, pp. 1098-1103, 2014.
[21] J. Sun, "Small-signal methods for ac distributed power systems – A Review," *IEEE Trans. Power Electron*., Vol. 24, No. 21, pp. 2545-2554, Nov. 2009.
[22] M. Huang, C K. Tse, S. C. Wong. "Hopf-type Bifurcation in Three-Phase PFC Power Supplies Connected to Non-ideal Power Grid," in *Proc. IWCFA*, pp. 151-154, 2012.
[23] M. Huang, C K. Tse, and S. C Wong, "Line-frequency Instability of Three-Phase PFC Power Supplies Connecting to Non-ideal Power Grid," in *Proc. IEEE ISCAS*., pp. 213-216, 2012.
[24] Z. Sütö, I. Nagy, "Analysis of Nonlinear Phenomena and Design Aspects of Three-Phase Space-Vector-Modulated Converters," *IEEE Trans. Circuit and Sys*., Vol. 50 No. 8, pp. 1064-1071, Aug. 2003.
[25] C. Xia, P. Song, T. Shi, and Y. Yan, "Chaotic Dynamics Characteristic Analysis for Matrix Converter," *IEEE Trans. Ind. Electron*., Vol. 60, No. 1, pp. 78-87, Jan. 2013.
[26] M. Huang, S. C. Wong, C K. Tse, and X. Ruan, "Catastrophic Bifurcation in Three-Phase Voltage-Source Converters," *IEEE Trans. Circuits Sys. I: Regular Papers*, Vol. 60, No.4, pp. 1062-1071, Apr. 2013.
[27] H. O. Wang, E. H. Abed, and A. M. Hamdan, "Bifurcations, chaos, and crises in voltage collapse of a model power system," *IEEE Trans. Circuits and Syst. - I: fundamental theory and applications*., Vol. 41, No. 3, pp. 294-302, Mar. 1994.
[28] H. G. Kwatny, A. Pasrija, and L. Bahar, "Static bifurcations in electric power networks: Loss of steady-state stability and voltage collapse," *IEEE Trans. Circuits and Syst*., Vol. 33, No. 10, pp. 981-991, Oct. 1986.
[29] C. S. Kong, "A General Maximum Power Transfer Theory," IEEE Trans. Education, Vol. 38, No. 3, pp. 296-298, Aug. 1995.

Chunguang Ren was born in China, in 1989. He received his B.S. degree from the Taiyuan University of Science and Technology, Taiyuan, China, in 2012. He is presently working towards his Ph.D. degree in Taiyuan University of Technology. His current research interests include power electronics interfaces for renewable energy sources in microgrids and the stability of power converters.

Huipeng Li was born in China, in 1985. He received his M.S. degree from the Taiyuan University of Technology, Taiyuan, China, in 2013. He is presently working as an Engineer at the Shanxi Electric Power Research Institute, Taiyuan, China. His current research interests include power electronics and control, power quality, and microgrid operation and control.

Yu Yang was born in China, in 1975. He received his Ph.D. degree from Xi'an Jiaotong University, Xi'an, China, in 2007. He is presently working as a Senior Engineer at the Shanxi Electric Power Corporation, Taiyuan, China. His current research interests include power electronics and control, power quality compensation systems, and nonlinear phenomena in power electronic circuits and systems.

Xiaoqing Han received her B.S., M.S. and Ph.D. degrees from the College of Electrical and Power Engineering, Taiyuan University of Technology, Taiyuan, China. She is presently working as a Professor at the Taiyuan University of Technology. Her current research interests include power system simulation, stability analysis, and the integration of renewable energy sources.

Peng Wang received his B.S. degree from Xi'an Jiaotong University, Xi'an, China, in 1978; his M.S. degree from the Taiyuan University of Technology, Taiyuan, China, in 1987; and his M.S. and Ph.D. degrees from the University of Saskatchewan, Saskatoon, SK, Canada, in 1995 and 1998, respectively. He is presently working as a Professor at the Nanyang Technological University, Singapore.